Practical Event Location Estimation Algorithm for Power Transmission System Based on Triangulation and Oscillation Intensity

Shengyuan Liu, *Graduate Student Member, IEEE*, Kaiqi Sun, *Member, IEEE*, Chujie Zeng, Shutang You, *Senior Member, IEEE*, Hongyu Li, Wenpeng Yu, Xianda Deng, *Member, IEEE*, Zhenzhi Lin, *Senior Member, IEEE*, and Yilu Liu, *Fellow, IEEE*

***Abstract*—Event location in power systems is quite essential information for system operators to enhance control-room situational awareness capability. Therefore, it is of great importance to develop an event location estimation algorithm for transmission systems with high accuracy. With the development of wide-area measurement system (WAMS) such as FNET/GridEye, and the synchrophasor measurement devices (SMDs) such as frequency disturbance recorders (FDRs), the synchronous measurement data including frequency, voltage amplitude and phase angle can be collected and used for event location estimation. First, the phase angle and rate of change of frequency (RoCoF) trajectories are respectively used for determining two sets of wave arrival time associated with each FDR. Then, a convolutional neural network (CNN) is utilized to determine the wave arrival order to select the more suitable set of wave arrival times for a given case and to perform corresponding modifications. Next, the oscillation intensity associated with each FDR is determined based on phase angle trajectories in the center of inertia (COI) coordinate system. Finally, the multiple criteria for event location estimation are represented. Case studies and comparisons between the proposed and previous algorithms using actual and confirmed cases in U.S. power systems are performed to demonstrate the effectiveness and improvement of the proposed algorithm in practical applications.**

***Index Terms*—Event location estimation, wave arrival time, convolutional neural network (CNN), oscillation intensity, triangulation, synchrophasor measurement, FNET/GridEye, frequency disturbance recorder (FDR).**

I. Introduction

ACCURATE event location estimation is of great importance for enhancing the capability of power system operators. As one of the most fundamental infrastructures for society and modern industry, the electric power system has witnessed continuous growth for its scale and complexity in decades with the economic growth [1]–[3]. In the meantime, the emergence of the wide-area measurement system (WAMS) brings an unprecedented way for system operators to achieve fast and accurate monitoring and control of power systems [4]–[6]. Since 2003, the frequency monitoring network, FNET/GridEye was been developed based on synchrophasor technologies [7], [8], and is currently operated by the University of Tennessee, Knoxville (UTK) and Oak Ridge National Laboratory (ORNL). In the past almost 20 years, the FNET/GridEye has provided many critical services, such as situation awareness, system operations, post-event analysis and compliance for the partners including utilities, balancing authorities (BAs), regional coordinators (RCs), electric reliability organizations (EROs), and the U.S. federal agencies. The contribution of FNET/GridEye is widely acknowledged by the power industry.

As one of the most important functions of the FNET/GridEye, the event location estimation has been developed and deployed to enhance the situational awareness ability of system operators. The real-time information measured from frequency disturbance recorders (FDRs) is used by FNET/GridEye to achieve online detection and location estimation of power system events so as to inform operators the information of events in real time and take corresponding responses. The basic principle of event location estimation applied in FNET/GridEye is triangulation based on the different wave arrival times among FDRs at different locations [9], [10]. Once the wave arrival time of three or more FDRs is obtained, the locations of the event can be estimated by solving equations using the least square method

Manuscript received 3 October 2021; revised 1 February 2022 and 19 April 2022; accepted 26 April 2022. Date of publication 12 May 2022; date of current version 28 November 2022. This work was supported by the NSF Cyber-Physical Systems (CPS) Program under Award 1931975. This work also made use of Engineering Research Center shared facilities supported in part by the Engineering Research Center Program of the National Science Foundation and the Department of Energy under NSF Award EEC-1041877, and in part by the CURENT Industry Partnership Program. Paper no. TPWRD-01468-2021. *(Corresponding author: Kaiqi Sun.)*

Shengyuan Liu is with the Department of Electrical Engineering and Computer Science, University of Tennessee, Knoxville, TN 37996 USA, and also with the School of Electrical Engineering, Zhejiang University, Hangzhou 310027, China (e-mail: eelsy@zju.edu.cn).

Kaiqi Sun is with the School of Electrical Engineering, Shandong University, Jinan 250061, China (e-mail: skq@sdu.edu.cn).

Zhenzhi Lin is with the School of Electrical Engineering, Zhejiang University, Hangzhou 310027, China, and also with the School of Electrical Engineering, Shandong University, Jinan 250061, China (e-mail: linzhenzhi@zju.edu.cn).

Chujie Zeng, Shutang You, Hongyu Li, Wenpeng Yu, and Xianda Deng are with the Department of Electrical Engineering and Computer Science, University of Tennessee, Knoxville, TN 37996 USA (e-mail: czeng8@utk.edu; syou3@utk.edu; hli90@utk.edu; wyu10@utk.edu; xdeng6@utk.edu).

Yilu Liu is with the Department of Electrical Engineering and Computer Science, University of Tennessee, Knoxville, TN 37996 USA, and also with the Oak Ridge National Laboratory, Oak Ridge, TN 37830 USA (e-mail: liu@utk.edu).

Color versions of one or more figures in this article are available at https://doi.org/10.1109/TPWRD.2022.3173974.

Digital Object Identifier 10.1109/TPWRD.2022.3173974

[11], [12]. However, accurate determination of wave arrival time is very difficult in actual applications, which would further influence the accuracy of location estimation. With the recent progress on the application of machine learning approaches in power systems, data-based system estimation applications have also been studied to improve the accuracy of event location estimation [13]–[15]. In [13], recurrence quantification analysis (RQA) is applied and the change rate of recurrence rate (RR) is utilized to show the buses near the event location. In [14], the short-time local outlier probability (ST-LOP)-based algorithm is utilized to detect and locate the events associated with distributed energy resources. In [15], the similarity search with the local outlier factor (SS-LOF)-based algorithm is further developed and can achieve higher accuracy for event location estimation with slightly longer computation time.

However, the aforementioned algorithms are simply model-based or data-based, while synthesizing them together could bring potential opportunities to further improve the performance. Given this background, this work proposes a hybrid estimation algorithm for event location based on traditional wave arrival time determination and its modification using a convolutional neural network (CNN), and oscillation intensity determination. Concretely, the term "events" in this work refers to generation trip (GT), load shedding (LS) and associated oscillations in power systems. The contributions of this work can be summarized as follows.

1) The wave arrival time is determined independently by utilizing the rate of change of frequency (RoCoF) and phase angle first, and then the CNN is utilized for determining the wave arrival order. Coincidence indexes are defined to select the more consistent one, and CNN helps to modify the wave arrival time of FDRs in sequence, which can greatly improve the accuracy of the final event location estimation result.
2) The oscillation intensities measured by FDRs located in different places are also investigated and they are employed to improve the estimation accuracy of event location especially for the severe events in power systems with large disturbances. Besides, it is the first time to combine multiple event location estimation criteria associated with triangulation and deep learning techniques for enhancing the performance of event location estimation to our best knowledge.
3) Demonstrations in actual U.S. power systems are performed and the actual measured data from FNET/ GridEye are utilized for batch verification. Compared with the existing algorithm deployed in FNET/ GirdEye, the proposed algorithm can reduce the average estimation error by 16.79%. Furthermore, the parameter selection and corresponding sensitivity analysis are performed in detail to increase the applicability of the proposed event location estimation algorithm.

The rest of this paper is organized as follows. The principle of the event location estimation algorithm deployed in FNET/GridEye based on wave arrival time determination and triangulation is briefly introduced in Section II. Section III introduces the hybrid algorithm for event location estimation based on oscillation intensity determination and wave arrival time modification using CNN. The verifications of the proposed methods using the actual measured data in the U.S. power system are conducted in Section IV, and the conclusions of this work are given in Section V.

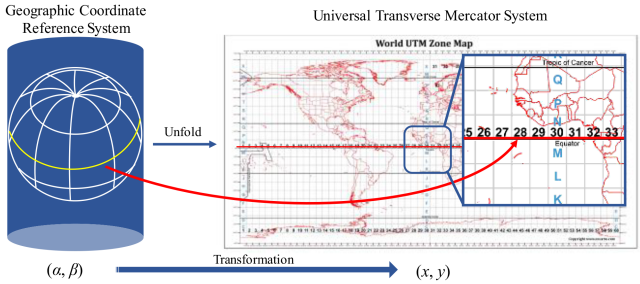

Fig. 1. Schematic diagram for coordinate system transformation.

II. Event Location Estimation Algorithm Based on Wave Arrival Time Determination and Triangulation

The basic principle of event location estimation based on triangulation is to utilize the different delays of the wave arrival time of FDRs at different locations to represent the corresponding distances between actual event location and FDRs. Theoretically, three FDRs are enough for triangulation while more FDRs are needed for the robustness of the estimation algorithm in practice. First, coordinate system transformation should be performed to avoid nonlinear triangulation equations. Then, the event detection criterion is represented, which is the prerequisite of event location estimation. Next, a wave arrival time determination method that serves for triangulation is introduced. Finally, the linear form of triangulation for event location estimation is given.

A. Mutual Transformation Between Geographic Coordinate Reference System and Universal Transverse Mercator Grid System

Generally, the geographic coordinate reference (GCR) system is used for the global position system (GPS), so the locations of deployed FDRs and the event location to be estimated are denoted as latitude and longitude coordinates. Therefore, the formula of the distance between the actual event location and the nth FDR will be in the nonlinear form as

$$D_n^{\mathrm{E}} = R\cos^{-1}[\sin\alpha_{\mathrm{E}}\sin\alpha_n + \cos\alpha_n\cos\alpha_{\mathrm{E}}\cos(\beta_n - \beta_{\mathrm{E}})] \tag{1}$$

where R is the radius of the earth; α_{E} and α_n are the latitudes of the actual event location and the nth FDR, respectively; β_{E} and β_n are their longitudes, respectively. To avoid solving nonlinear equations in Section II–D, the latitude and longitude coordinates in the GCR system are required to be transformed into x-y coordinates in the universal transverse Mercator (UTM) grid system as shown in Fig. 1. Denote x and y as the horizontal and vertical coordinates in the UTM system, and α and β as

the latitude and longitude coordinates in the GCR system. The transformation [16] and [17] from the GCR system to the UTM system could be expressed as follows.

$$\begin{cases} x = x_0 + k_0 S[\rho_L{}' + \sum_{j=1}^{3} \varphi_j \cos(2j\xi_L{}') \sinh(2j\rho_L{}')] \\ y = y_0 + k_0 S[\xi_L{}' + \sum_{j=1}^{3} \varphi_j \cos(2j\xi_L{}') \cosh(2j\rho_L{}')] \end{cases} \tag{2}$$

where

$$\begin{cases} \xi_L{}' = \tan^{-1}[\frac{q}{\cos(\beta-\beta_0)}] \ \rho_L{}' = \tanh^{-1}[\frac{\sin(\beta-\beta_0)}{\sqrt{1+q^2}}] \\ q = \sinh[\tanh^{-1}\sin\alpha - \frac{2\sqrt{w}}{1+w}\tanh^{-1}(\frac{2\sqrt{w}}{1+w}\sin\alpha)] \\ \varphi_1 = \frac{1}{2}w - \frac{2}{3}w^2 + \frac{5}{16}w^3 \ \varphi_2 = \frac{13}{48}w^2 - \frac{3}{5}w^3 \ \varphi_3 = \frac{61}{240}w^3 \\ S = \frac{R}{1+w}(1 + \frac{w^2}{4} + \frac{w^4}{64} + \cdots) \quad w = \frac{f}{2-f} \end{cases} \tag{3}$$

where x_0 is false northing and $x_0 = 0$ for all zones in the northern hemisphere. y_0 is false easting and $y_0 = 500$ for every zone. β_0 is the longitude of the prime meridian and $\beta_0 = 0$. R is the radius of earth and $R = 6378.137$. f is the flattening of earth and $f = 3.35381\times10^{-3}$. k_0 is the scale factor associated with the distance from the central meridian of the projection and its typical value is 0.9996.

The transformation between GCR system and UTM system would cause up to 0.1% error [16], which is accurate enough for this work. Once the latitude and longitude coordinates are transformed into x-y coordinates, the distance between the actual event location and the nth FDR be can obtained by

$$D_n^{\mathrm{E}} = \sqrt{(x_{\mathrm{E}} - x_n)^2 + (y_{\mathrm{E}} - y_n)^2} \tag{4}$$

Thus, the strongly nonlinear operators $\sin(\bullet)$, $\cos(\bullet)$, and $\cos^{-1}(\bullet)$ in (1) are eliminated and (4) can be easily reformulated into the linear form which will be further discussed in Section II–D. After determining the final event location, the x-y coordinates can be transformed back to latitude and longitude coordinates by

$$\begin{cases} \alpha = \chi + \sum_{j=1}^{3} \delta_j \sin(2j\chi) \\ \beta = Z_{\mathrm{zone}} \times 6^\circ - 183^\circ + \tan^{-1}(\sinh\rho_U{}' / \cos\xi_U{}') \end{cases} \tag{5}$$

where

$$\begin{cases} \xi_U{}' = \xi_U - \sum_{j=1}^{3} \lambda_j \sin(2j\xi_U) \cosh(2j\eta_U) \\ \rho_U{}' = \rho_U - \sum_{j=1}^{3} \lambda_j \cos(2j\xi_U) \sinh(2j\rho_U) \\ \lambda_1 = \frac{1}{2}w - \frac{2}{3}w^2 + \frac{37}{96}w^3 \ \lambda_2 = \frac{1}{48}w^2 + \frac{1}{15}w^3 \ \lambda_3 = \frac{17}{480}w^3 \\ \xi_U = \frac{x-x_0}{k_0 S}\rho_U = \frac{y-y_0}{k_0 S} \\ \chi = \sin^{-1}(\frac{\sin\xi_U{}'}{\cosh\rho_U{}'}) \end{cases} \tag{6}$$

where $\mathrm{Z_{zone}} \in [1, 60]$ is the current code of UTM zones, which is related to the study area.

B. Event Detection Trigger in FNET/GridEye Based on the RoCoF

FNET/GridEye is a pilot wide-area phasor measurement system that can cover the national level power grid at a low cost. FDRs in the FNET/GridEye transmit the collected phasor measurements to the data center located at the UTK and ORNL. The FNET/GridEye data center employs a multi-layer architecture as shown in Fig. 2, and it is designed to receive, process, and archive real-time synchrophasor measurements [18]. In this work, the frequency data, phase angle data, and voltage amplitude data are taken from the FNET/GridEye for event location and they are all real-time synchrophasor measurements with a 10Hz reporting rate.

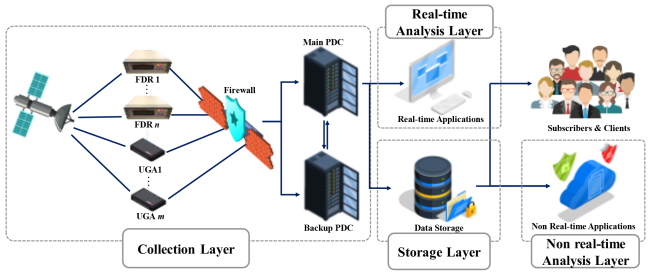

Fig. 2. Structure of the FNET/GridEye data center.

For a detected event in power systems, the aforementioned data of N FDRs would be archived with the T time window with 10 Hz resolution. They can be denoted as

$$\mathbf{L}^{\mathrm{Data}} = \{\mathbf{L}_{N\times T}^{\mathrm{Fre}}, \mathbf{L}_{N\times T}^{\mathrm{Ang}}, \mathbf{L}_{N\times T}^{\mathrm{Amp}}\} \tag{7}$$

Since noises exist in measurement data, it would be better to narrow the window for wave arrival time determination as short as possible. Therefore, a rough event time should be obtained first for further analysis, which is also the prerequisite for wave arrival time determination. The steps of real-time event detection can be briefly summarized as follows.

Step 1: Denoise the recorded frequency data by the median filter and save them in a buffer for further analysis.

Step 2: Determine the RoCoF of the nth FDR (n = 1, 2, …, N_{FDR}) at time t as

$$L_{n,t}^{\mathrm{RoCoF}} = \frac{L_{n,t+N_{\mathrm{win}}}^{\mathrm{Fre}} - L_{n,t}^{\mathrm{Fre}}}{N_{\mathrm{win}}} \quad (n = 1, 2, \ldots, N_{\mathrm{FDR}}) \tag{8}$$

where N_{FDR} is the number of FDR available online and N_{win} is the window length (i.e., number of sample points) for the RoCoF. $L_{n,t+N_{\mathrm{win}}}^{\mathrm{Fre}}$ and $L_{n,t}^{\mathrm{Fre}}$ are the frequency data of the nth FDR (n = 1, 2, …, N_{FDR}) at time t+N_{win} and time t, respectively. In actual applications, N_{win} is selected as 6 according to experience for avoiding noise and obtaining more robust results. To illustrate the influence of this parameter, corresponding sensitivity analysis is performed in Section V.

Step 3: If more than N_τ FDRs satisfy the inequation (9), the event is detected and the event time is determined as t_{E}

$$|L_{n,t_{\mathrm{E}}}^{\mathrm{RoCoF}}| > \tau \quad (n = 1, 2, \ldots, N_{\mathrm{FDR}}) \tag{9}$$

where N_τ and τ are the thresholds used for event detection and can be tuned by past events. To illustrate the influence of these thresholds, the corresponding sensitivity analysis is also performed in Section V.

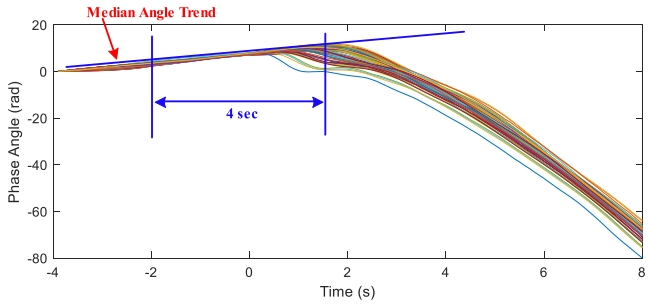

Fig. 3. Monotonic increasing or decreasing trend before the disturbance.

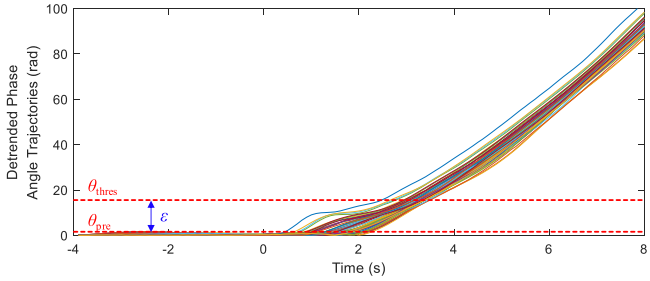

Fig. 4. Wave arrival time determination based on detrended phase angle trajectories.

C. Wave Arrival Time Determination for FDRs Located in Different Places Based on Phase Angle Trajectories

After an event is detected by FNET/GridEye, the wave arrival time for each FDR (i.e., t_n, $n = 1, 2, \ldots, N_{\mathrm{FDR}}$) can be determined based on phase angle trajectories. As shown in Fig. 3, there usually exists a monotonic increasing or decreasing trend before the disturbance, and such a trend needs to be removed. It is noted that the initial phase angle values of all FDRs are shifted to 0 in Fig. 3 for better illustrations. In this work, the system median angle curve within 4 seconds [19] before the disturbance is used to construct the trend. As a straight line, the trend crosses the middle point of the median angle curve and has the same slope. The detrended angle trajectories are shown in Fig. 4 and the trend is deducted from each phase angle curve.

For each FDR, its wave arrival time based on phase angle trajectories can be determined as the point when its detrended angle trajectory exceeds a certain threshold. As shown in Fig. 4, the threshold is set as the sum of a confidence parameter ε and the average value θ_{pre} of detrended angle trajectories before disturbances. Three seconds before the disturbance is used to determine the pre-disturbance average angle θ_{pre}, while the confidence parameter ε ε is fixed within the range from 0.8 to 3.2, which is empirically justified by historical cases in FNET/GridEye [19]. Then the final threshold is defined as

$$\theta_{\mathrm{thres}} = \theta_{\mathrm{pre}} + \varepsilon \tag{10}$$

Thus, the wave arrival time of each FDR (i.e., $t_n, n = 1, 2, \ldots, N_{\mathrm{FDR}}$) is determined as the first time that its detrended phase angle trajectory exceeds the threshold.

D. Event Location Estimation Based on Triangulation

Once the wave arrival time of each FDR is determined, the following equations can be obtained based on the relationship between distance and the time delay of wave travel.

$$\begin{cases} (x_1 - x_{\mathrm{E}})^2 + (y_1 - y_{\mathrm{E}})^2 = v^2(t_1 - t_{\mathrm{E}})^2 \\ (x_2 - x_{\mathrm{E}})^2 + (y_2 - y_{\mathrm{E}})^2 = v^2(t_2 - t_{\mathrm{E}})^2 \\ \vdots \\ (x_{N_{\mathrm{T}}} - x_{\mathrm{E}})^2 + (y_{N_{\mathrm{T}}} - y_{\mathrm{E}})^2 = v^2(t_{N_{\mathrm{T}}} - t_{\mathrm{E}})^2 \end{cases} \tag{11}$$

where v is average wave travel speed and is assumed as a uniform value for different directions; N_{T} is the number of FDRs employed for triangulation ($3 \le N_{\mathrm{T}} \le N_{\mathrm{FDR}}$). Subtract the adjacent equations in (11), several linear equations can be obtained as

$$\begin{cases} (x_{n+1} - x_n)x_{\mathrm{E}} + (y_{n+1} - y_n)y_{\mathrm{E}} - v^2(t_{n+1} - t_n)t_{\mathrm{E}} = c_n \\ (x_1 - x_{N_{\mathrm{T}}})x_{\mathrm{E}} + (y_1 - y_{N_{\mathrm{T}}})y_{\mathrm{E}} - v^2(t_1 - t_{N_{\mathrm{T}}})t_{\mathrm{E}} = c_{N_{\mathrm{T}}} \end{cases} \\ n = 1, 2, \ldots, N_{\mathrm{T}} - 1 \tag{12}$$

where c_n and $c_{N_{\mathrm{T}}}$ are constants and their values are

$$\begin{cases} c_n = \frac{1}{2}[v^2(t_{n+1} - t_n) + x_{n+1}^2 + y_{n+1}^2 - x_n - y_n] \\ c_{N_{\mathrm{T}}} = \frac{1}{2}[v^2(t_1 - t_{N_{\mathrm{T}}}) + x_{N_{\mathrm{T}}+1}^2 + y_{N_{\mathrm{T}}+1}^2 - x_{N_{\mathrm{T}}} - y_{N_{\mathrm{T}}}] \end{cases} \tag{13}$$

It can be seen from (12) and (13) that x_{E}, y_{E} and t_{E} are the variables to be solved and all other variables are known. Concretely, the locations of each FDRs (i.e., x_n and y_n, $n = 1, 2, \ldots, N_{\mathrm{T}}$) can be obtained in advance, the wave arrival time (i.e., t_n, $n = 1, 2, \ldots, N_{\mathrm{T}}$) can be determined by Equation (10). Therefore, these equations can be solved by the least square method by

$$\hat{\boldsymbol{\psi}} = (\mathbf{A}^{\mathrm{T}}\mathbf{A})^{-1}\mathbf{A}^{\mathrm{T}}\boldsymbol{c} \tag{14}$$

where $\hat{\boldsymbol{\psi}} = [\hat{x}_{\mathrm{E}}, \hat{y}_{\mathrm{E}}, \hat{t}_{\mathrm{E}}]^{\mathrm{T}}$, $\boldsymbol{c} = [c_1, c_2, \ldots, c_{N_{\mathrm{T}}}]^{\mathrm{T}}$ and

$$\mathbf{A} = \begin{bmatrix} x_2 - x_1 & y_2 - y_1 & -v^2(t_2 - t_1) \\ x_3 - x_2 & y_3 - y_2 & -v^2(t_3 - t_2) \\ \vdots & \vdots & \vdots \\ x_1 - x_{N_{\mathrm{T}}} & y_1 - y_{N_{\mathrm{T}}} & -v^2(t_1 - t_{N_{\mathrm{T}}}) \end{bmatrix} \tag{15}$$

It should be mentioned that the N_{T} should be equal to or larger than 3, which can be either explained from a physical or mathematical perspective. From the physical perspective, at least three measurement points and corresponding distance can uniquely locate the source point in 2D plane. From the mathematical perspective, the rank of the product of two matrices is smaller than either of them according to the theory of linear algebra. $\mathbf{A}$ is a $N_{\mathrm{T}} \times 3$ dimensional matrix and $\mathbf{A}^{\mathrm{T}}\mathbf{A}$ is a 3×3 dimensional matrix. Therefore, N_{T} is required to be 3 or larger so that $\mathbf{A}^{\mathrm{T}}\mathbf{A}$ can be a full rank matrix and $(\mathbf{A}^{\mathrm{T}}\mathbf{A})^{-1}$ in Equation (14) can be solved.

In practical applications, N_{T} will be iterated from 3 to 10 and the final result is determined with the least fitting residuals. The fitting residuals can be denoted as

$$e_{\mathrm{E}} = \sum_{n=1}^{N_{\mathrm{T}}} (x_n - \hat{x}_{\mathrm{E}})^2 + (y_n - \hat{y}_{\mathrm{E}})^2 + (t_n - \hat{t}_{\mathrm{E}})^2 \tag{16}$$

It is also worth mentioning that the principle of selecting FDRs is to select the FDRs with the earliest N_{T} wave arrival times. After the final $\hat{x}_{\mathrm{E}}$ and $\hat{y}_{\mathrm{E}}$ are determined, the latitude and longitude of the event $\hat{\alpha}_{\mathrm{E}}$ and $\hat{\beta}_{\mathrm{E}}$ can be determined as well by coordinate system transformation mentioned in Section II–A.

III. Hybrid Algorithm for Event Location Estimation

During the applications of the algorithm mentioned in Section II, it is found that the estimation errors are still very large for several cases (e.g., >800 miles). The most critical reason could be that the system frequency wave is the electromechanical wave whose speed is different for different directions. Therefore, assuming v as a uniform value would cause errors. However, if the v is set as an anisotropic variable, then (11) would be the underdetermined system of equations and the solution of event location cannot be obtained. Therefore, the variable v is still assumed as a constant in this work and a new hybrid event location estimation algorithm is presented in this section for further mitigating the location estimation errors as small as possible. Compared with existing ones, the new algorithm: i) considers the oscillation intensity as an auxiliary criterion for the severe events; ii) takes both the phase angle data and the RoCoF data for wave arrival time determination, and a CNN structure is proposed for further time modification.

A. Oscillation Intensity Determination of Events

In fact, considerable phase angle variations would be caused when major events happen in power systems. Therefore, these characteristics can be utilized to boost the performance of event location estimation.

It should be mentioned that i) the initial phase angles of different buses are already different which is hard to measure the oscillation intensity differences among different places intuitively; and ii) a reference phase angle trajectory is needed for determining the oscillation intensity in different places while how to automatically select a suitable reference trajectory should be taken into consideration. For the first issue, it can be solved by subtracting the value of the first point (i.e., $L_{n,1}^{\mathrm{Ang}}$) from the subsequent values, which can be represented as

$$L_{n,t}^{\mathrm{Ang}'} = L_{n,t}^{\mathrm{Ang}} - L_{n,1}^{\mathrm{Ang}} \tag{17}$$

where $L_{n,t}^{\mathrm{Ang}}$ and $L_{n,1}^{\mathrm{Ang}}$ are the phase angle data of the nth FDR at time t and the beginning point of the event (i.e., t_{E} in (9)), respectively. For the second issue, the concept of center of inertia (COI) can be utilized, and all phase angle trajectories can be transformed into COI coordinate system, i.e.,

$$L_{n,t}^{\mathrm{AngCOI}} = L_{n,t}^{\mathrm{Ang}'} - L_{\mathrm{COI}}^{\mathrm{Ang}} \tag{18}$$

where $L_{\mathrm{COI}}^{\mathrm{Ang}}$ is the COI for the phase angle and can be calculated as

$$L_{\mathrm{COI}}^{\mathrm{Ang}} = \sum_{n=1}^{N} H_n L_{n,t}^{\mathrm{Ang}'} / \sum_{n=1}^{N} H_n \tag{19}$$

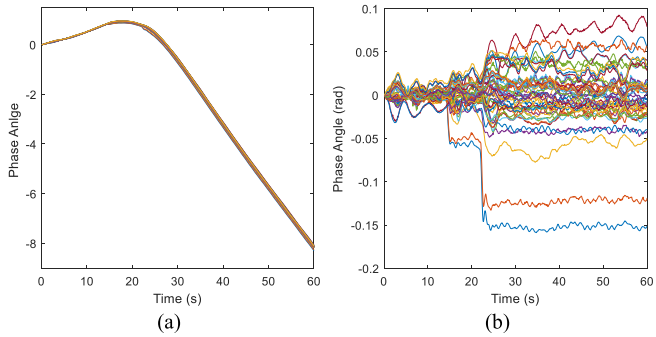

Fig. 5. Illustration of phase angle trajectories. (a) Original coordinate system; (b) COI coordinate system.

where H_n is the inertia near the nth FDR and can be estimated by the method introduced in our previous work [20] using synchrophasor measurement data at multiple locations. Sometimes, it is hard to estimate the value of H_n. In these situations, the values of all H_n ($n = 12, \ldots, N$) can be regarded as the same value, and then (18) would be degraded into

$$L_{n,t}^{\mathrm{AngCOI}} = L_{n,t}^{\mathrm{Ang}'} - \frac{1}{N}\sum_{n=1}^{N} L_{n,t}^{\mathrm{Ang}'} \tag{20}$$

An illustration of the phase angle trajectories in the original coordinate system and COI coordinate system is shown in Fig. 5. It can be seen that it difficult to measure the relative angle differences among different trajectories intuitively in Fig. 5(a), while it will be more vivid if using Fig. 5(b). Therefore, the oscillation intensity of the event near the nth FDR can be defined as

$$I_n = \max_{1\le t\le T}\left\{L_{n,t}^{\mathrm{AngCOI}}\right\} - \min_{1\le t\le T}\left\{L_{n,t}^{\mathrm{AngCOI}}\right\} \tag{21}$$

The oscillation intensity describes the extent of phase angle variation and can be used for characterizing the distance between the actual event location and the given FDR. Generally, the higher the I_n is, the shorter the distance between the actual event location and the nth FDR is. However, in actual applications, it is found that using wave arrival time to determine the distance is more accurate than using oscillation for most cases. Indeed, the idea of incorporating the intensity into the event location estimation is empirical and it is based on the evidence that severe events would lead the large oscillations of phase angle near the event location. Generally, the larger the oscillations, the nearer the event location to the measurement devices. To avoid the misapplications of the oscillation intensity-based method, the oscillation intensity is only used as an auxiliary criterion and is designed for the severe events that happen in power systems that cause large oscillation. For these situations with severe events, a parameter η is also defined for deciding whether trigger this criterion and the effectiveness of the oscillation intensity-based criterion will be shown in Sections IV–B and V–C, which achieves quite good results.

B. Wave Arrival Time Modification Based on CNN

Since the wave arrival time determination method based on phase angle as given in (10) is not quite accurate in some cases in practice, another wave arrival time determination method based on RoCoF is also represented as a supplement. In addition, a CNN structure is utilized to decide which one should be used and to give corresponding modifications for a certain case. The rationale and necessity of using CNN for determining wave arrival order are as follows.

1) Both the wave arrival time determination method based on phase angle trajectories and RoCoF require the subjective engineering experience and different wave arriving times may be obtained by them, which need additional modification.
2) CNN structure only needs the objective measurement data as the inputs to determine the wave arrival order by comparing each data pair, and the measurement data in the whole time interval are utilized, which can give more comprehensive results.
3) CNN structure can only determine the wave arrival order since the ground truth of event time cannot be known and cannot be utilized for training. Therefore, the wave arrival time is determined based on phase angle trajectories and RoCoF first and is modified based on the CNN model after that.

In fact, the rate of change of frequency (RoCoF) is the time derivative of the power system frequency and has been utilized for power system relay [21], event detection [22] or event classification [23] recently. The effectiveness of using RoCoF has been demonstrated in the literature. As the derivative of the frequency signal, RoCoF is more sensitive to the frequency change in power systems when compared with frequency data itself and can detect the power system event or perform frequency relay much faster. The wave arrival time based on RoCoF can be determined as the first time t that satisfies (22) for generation trip events and (23) for load shedding events.

$$L_{n,t}^{\mathrm{RoCoF}} \le \max\left\{\min_{t_{\mathrm{E}}-t_{\mathrm{pre}}\le t\le t_{\mathrm{E}}+t_{\mathrm{post}}}\left\{L_{n,t}^{\mathrm{RoCoF}}\right\},\zeta_1\right\} \tag{22}$$

$$L_{n,t}^{\mathrm{RoCoF}} \ge \min\left\{\max_{t_{\mathrm{E}}-t_{\mathrm{pre}}\le t\le t_{\mathrm{E}}+t_{\mathrm{post}}}\left\{L_{n,t}^{\mathrm{RoCoF}}\right\},\zeta_2\right\} \tag{23}$$

where t_{pre} and t_{post} are the times before and after the event occurs, respectively; ζ_1 and ζ_2 are parameters and has been tuned as -0.015 and 0.015 by past events, respectively. To illustrate the influence of these thresholds, the corresponding sensitivity analysis is performed in Section V.

In brief, the CNN-based time modification is developed by determining the wave arrival order. Because the number of available FDRs in each event is uncertain, the order is determined in a pairwise manner for better flexibility and robustness. The inputs of the proposed CNN-based model are the frequency data from two FDRs to be compared, and the outputs of the proposed CNN-based model are the results (i.e., 0 or 1) that denote which FDR wins. Therefore, each time the CNN model compares two FDRs to determine their relative wave arrival order as shown in Fig. 6. For an event with N_{FDR} available FDRs, N_{FDR}(N_{FDR}-1)

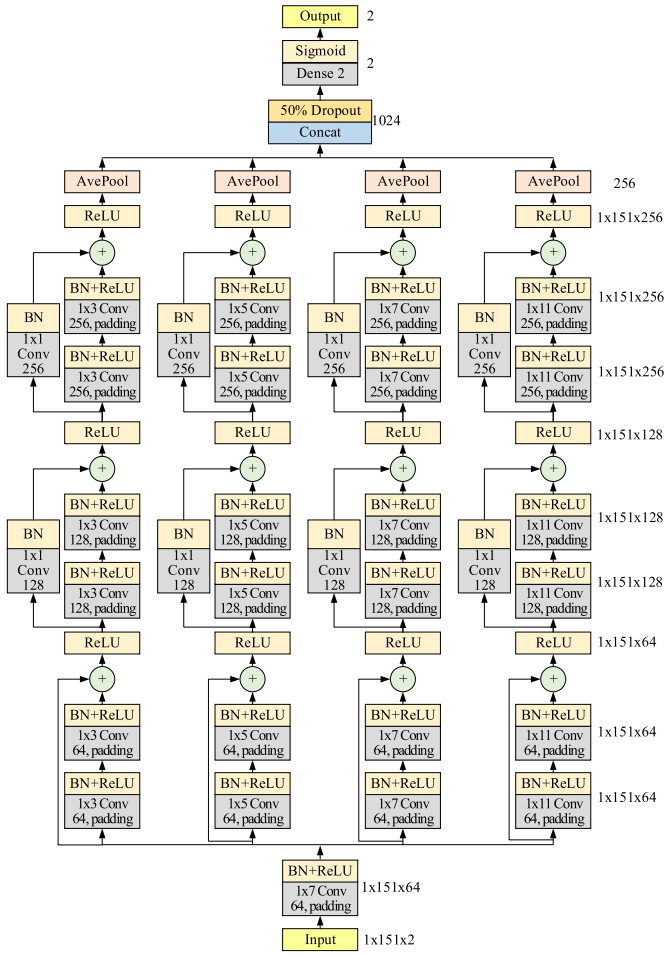

Fig. 6. CNN structure for wave arrival time modification.

comparisons would be performed and the Borda count method [24] is applied to aggregate pairwise orders into the order of all FDRs.

Let Γ_i^k represents the outcome of the kth comparison for the ith FDR, then it can be denoted as

$$\Gamma_i^k = \begin{cases} 1, & \text{if the } i\text{th FDR wins in the } k\text{th comparison} \\ 0, & \text{otherwise} \end{cases} \tag{24}$$

Therefore, the quantity $N_i^{\Gamma} = \sum_k \Gamma_i^k$ corresponds to the number of comparisons that the ith FDR wins. The wave arrival order of all FDRs then is derived from the descending order of their numbers of pairwise wins. In other words, the first FDR in wave arrival order has the largest number of wins, the second FDR has the second largest number of wins, and the rest are similar. Thus, although the wave arrival time cannot be obtained by the proposed CNN model, the wave arrival order can be determined and can be denoted as W_n^{CNN} ($n = 1, 2, \ldots, N_{\mathrm{FDR}}$). However, the judgment on the coincidence of RoCoF and phase angle results with the CNN ordering is inconvenient based on observation. Therefore, a proper coincidence index should be defined. Assume that the wave arrival time determined by phase angle and RoCoF are denoted as t_n^{Ang} and t_n^{RoCoF}, and the corresponding order are denoted as W_n^{Ang} and W_n^{RoCoF} ($n =$

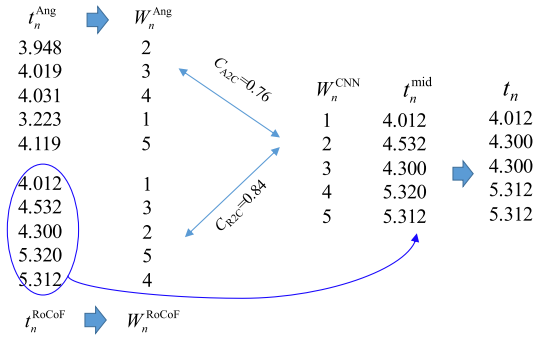

Fig. 7. An example for the wave arrival time modification based on the CNN model.

$1, 2, \ldots, N_{\text{FDR}}$), then the coincidence indexes can be defined as

$$C_{\text{A2C}} = 1 - \frac{\sum_{n=1}^{N_{\text{FDR}}} |W_n^{\text{Ang}} - W_n^{\text{CNN}}|}{N_{\text{FDR}}^2} \tag{25}$$

$$C_{\text{R2C}} = 1 - \frac{\sum_{n=1}^{N_{\text{FDR}}} |W_n^{\text{RoCoF}} - W_n^{\text{CNN}}|}{N_{\text{FDR}}^2} \tag{26}$$

where C_{A2C} and C_{R2C} respectively denote the consistency between W_n^{Ang} and W_n^{CNN} and the consistency between W_n^{RoCoF} and W_n^{CNN}. If $C_{\text{A2C}} > C_{\text{R2C}}$, then W_n^{Ang} is more consistent with W_n^{CNN}; otherwise, W_n^{RoCoF} is more consistent with W_n^{CNN}. Next, the more consistent one's wave arrival time would be utilized and is denoted as t_n^{mid}. (i.e., t_n^{Ang} or t_n^{RoCoF}). It should be noted that although the order of t_n^{mid} is more consistent with W_n^{CNN}, there still are some differences. Hence, the t_n^{mid} should be further modified as

$$t_n = \min\left\{t_n^{\text{mid}}, t_{W_n^{\text{CNN}}}^{\text{mid}}\right\} \quad n = 1, 2, \ldots, N_{\text{FDR}} \tag{27}$$

so as to avoid the situation that the FDRs with the front order are with the late wave arrival time. For example, if $N_{\text{FDR}} = 5$ and the t_n^{Ang}, t_n^{RoCoF} and W_n^{CNN} determined are shown in Fig. 7.

From t_n^{Ang} are t_n^{RoCoF}, W_n^{Ang} and W_n^{CNN} can be determined and compared with W_n^{CNN}. Since $C_{\text{A2C}} < C_{\text{R2C}}$, t_n^{RoCoF} is taken as t_n^{mid}. It can be seen that $t_2^{\text{mid}} > t_3^{\text{mid}}$ and $t_4^{\text{mid}} > t_5^{\text{mid}}$, which are conflict with the W_n^{CNN}. Therefore, t_2^{mid} is further modified and $t_2 = t_3^{\text{mid}} = 4.300$; t_4^{mid} is further modified and $t_4 = t_5^{\text{mid}} = 5.312$.

C. Comprehensive Event Location Estimation Algorithm With Multiple Criteria Considered for Practical Applications

In fact, a single criterion cannot achieve good performance in practical applications due to the measurement data quality, communication delay and unexpected errors. Therefore, it is of great necessity to pre-process the measured data first and then combine multiple estimation criteria together so as to reduce the errors of final event location estimation. The flowchart of the proposed hybrid event location estimation algorithm is shown in Fig. 8, and there are three stages as follows.

i) Data pre-processing;
ii) Wave arrival time and oscillation intensity determinations;

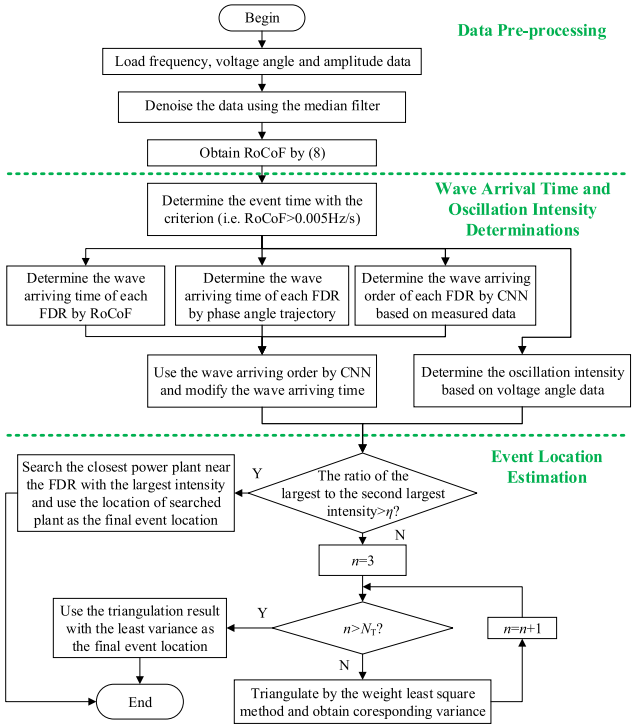

Fig. 8. Flowchart of proposed hybrid algorithm.

iii) Event location estimation.

In the first stage, the measured data are denoised and smoothed by using the median filter, and the RoCoF is obtained by (8). In the second stage, the two different sets of wave arrival time are respectively determined by phase angle and RoCoF, and CNN is employed for selecting the set of wave arrival time for a given case and giving corresponding modifications. In the meantime, the oscillation intensity near each FDR is determined based on phase angle data in COI coordinate system. In the last stage, multiple criteria are used to estimate the event location for a given case comprehensively. Concretely, if the difference of oscillation intensity between the largest and the second-largest exceeds a given threshold η, the event location will be estimated as the location of the power plant that is nearest to the FDR with the largest oscillation intensity; otherwise, the event location will be estimated by triangulation based on the differences among wave arrival time that is determined by phase angle, RoCoF, and CNN modification. In the estimation process, the number of FDRs (i.e., N_{T}) will be iterated from 3 to 10 to find the result with the least variance.

IV. Case Studies

To verify the effectiveness of the proposed algorithm, the actual measured and confirmed cases are utilized in this section for demonstrations and comparisons. Concretely, Case 1 is mainly utilized to illustrate the effectiveness of the criterion based on wave arrival time determination and CNN modification; Case 2 is mainly utilized to illustrate the effectiveness of the criterion based on oscillation intensity. In addition, the test performed on

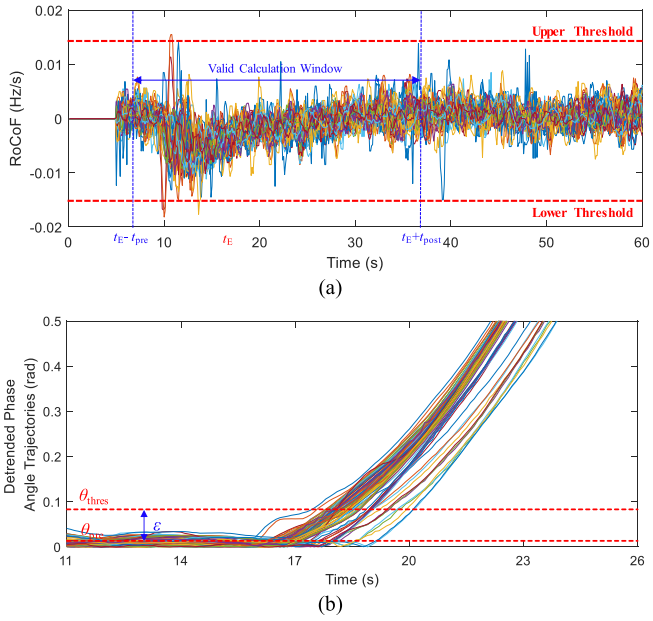

Fig. 9. RoCoF and detrended phase angle trajectories of Case 1. (a) RoCoF trajectories; (b) Detrended phase angle trajectories.

a large number of cases is also given to show the improvement of the proposed algorithm when compared with the previous one. It should be clarified that almost 800 events have been recorded by FNET/GridEye in the past and some of them are confirmed by power companies (e.g., North American Electric Reliability Corporation (NERC)), and the CNN model has been trained by them. Concretely, 80% of confirmed cases are utilized to train the CNN model, and the rest of them are utilized in work for testing the performance of the proposed hybrid event location estimation algorithm. Since the data are collected by deployed FDRs, the data arrival rate (i.e., data reporting rate) of this work is 10Hz, i.e., 10 points per second. Furthermore, the GPS coordinates of each FDR and the GPS coordinates of each power plant are the network data required for the analysis of this work.

A. Case 1: Generation Trip Occurs in Michigan

At 2019-10-19 21:59:03 UTC, a generation trip event in Michigan was detected by FNET/GridEye and this case is taken as an example of the aforementioned wave arrival time and order determination methods. In this case, the criterion based on oscillation intensity is not triggered, so only the trajectories of RoCoF and detrended phase angle are shown in Fig. 9, respectively. Based on the pre-tuned thresholds, the wave arrival time of each FDR determined by phase angle and RoCoF is given in Table I. Besides, the wave arrival order determined based on CNN is also given. It can be seen from Table I that the wave arrival time determined based on RoCoF is more consistent with the order determined based on CNN. Therefore, the wave arrival times determined by RoCoF are used for this case. It is worth mentioning the wave arrival time of *UsNyLewiston1436* (i.e., 21:59:04.500) is later than the one of *UsNyLeroy985* (i.e., 21:59:04.300). Thus, the wave arrival time of *UsNyLewiston1436* will be modified as 21:59:04.300 in practice and the final wave arrival time of each FDR is given in the last column of Table I.

TABLE I
RESULTS OBTAINED BY PHASE ANGLE-BASED AND ROCOF-BASED WAVE ARRIVAL TIME DETERMINATION AS WELL AS THE CNN-BASED ARRIVAL ORDER DETERMINATION FOR CASE 1

FDR Name	t_n^{Ang}	t_n^{RoCoF}	Order	Final t_n
UsOhAkron998	21:59:03.948	21:59:04.000	1	21:59:04.000
UsNyLewiston1436	21:59:04.019	21:59:04.500	2	21:59:04.300
UsNyLeroy985	21:59:04.031	21:59:04.300	3	21:59:04.300
CaOnToronto703	21:59:01.323	21:59:05.300	4	21:59:05.300
UsOhChilliecothe670	21:59:04.119	21:59:05.300	5	21:59:05.300
…	…	…	…	…

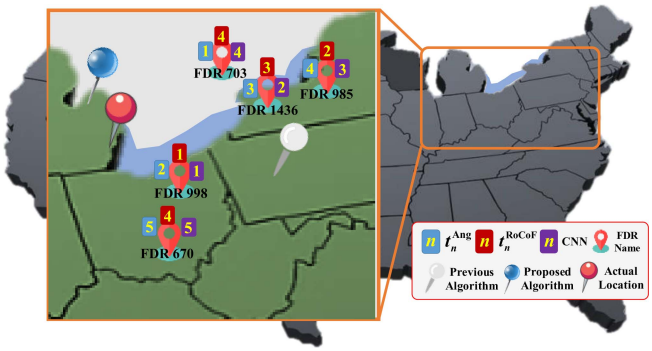

Fig. 10. Results of the phase angle-based and RoCoF-based wave arrival time and CNN-based wave arrival order.

TABLE II
COMPARISONS WITH THE PREVIOUS ALGORITHM FOR CASE 1

Previous Algorithm [11], [19]		Proposed Algorithm	
Estimated Location	Error	Estimated Location	Error
(40.7506, −78.4953)	265.78mi	(43.6103, −83.4856)	92.21mi

Actual Location: (42.304845, −83.152733).

In Fig. 10, the blue and red rectangles respectively indicate the first 5 FDRs selected by the previous location estimation algorithm and the proposed hybrid algorithm, and the number indicates its order, while the numbers in purple ones indicate the order determined by CNN. The actual event location is (42.304845, −83.152733), which is denoted as the red pin in Fig. 10. It can be seen that the proposed hybrid algorithm is more accurate with regard to the wave arrival order. The final estimated locations determined by the previous and proposed hybrid algorithms are given in Table II and shown in Fig. 10 as the white and blue pins, respectively. It can be seen that the proposed hybrid algorithm reduces the error from 265.78 mi to 92.21 mi when compared with the previous algorithm.

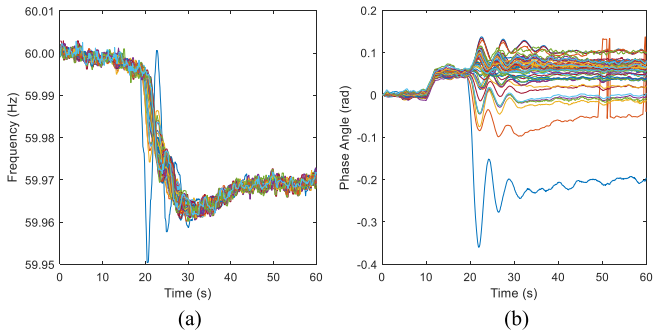

Fig. 11. Frequency and COI phase angle trajectories of Case 2. (a) Frequency trajectories; (b) COI phase angle trajectories.

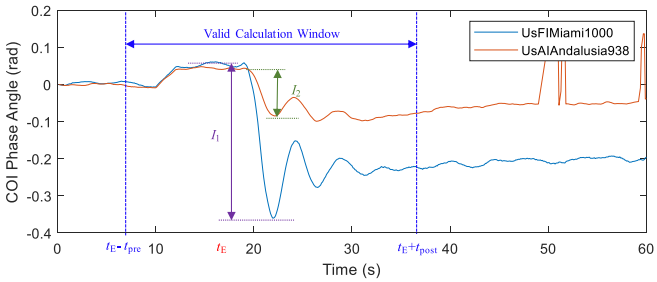

Fig. 12. Oscillation intensity determined for Case 2.

TABLE III
COMPARISONS WITH THE PREVIOUS ALGORITHM FOR CASE 2

Previous Algorithm [11], [19]		Proposed Algorithm	
Estimated Location	Error	Estimated Location	Error
(26.6967, -81.7831)	87.51mi	(26.0686, -80.1984)	44.98mi

Actual Location: (26.6986, -80.3747).

B. Case 2: Generation Trip Event Occurs in Florida

At 2018-01-12 21:53:10 UTC, a generation trip event in Florida was detected by FNET/GridEye, and the corresponding frequency and COI phase angle trajectories are shown in Fig. 11. Besides, the COI phase angle trajectories of the FDRs with the largest and the second-largest oscillation intensities (i.e., *UsFIMiami1000* and *UsAIAndalusia938*) are shown in Fig. 12. It can be seen that $I_1/I_2 > \eta = 1.3$, so the oscillation intensity-based criterion is activated and the event location is estimated at the closest power plant near FDR *UsFIMiami1000*. The final estimation results obtained by the previous algorithm and the proposed algorithm are given in Table III, and it can be seen that the proposed algorithm can achieve much smaller error (i.e., reducing the error from 87.51 mi to 44.98 mi), which demonstrates the effectiveness of the oscillation intensity-based criterion.

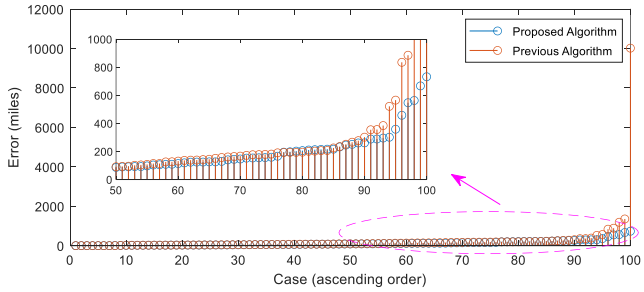

Fig. 13. Comparisons between the proposed and previous algorithms.

TABLE IV
STATISTICS OF ERRORS FOR BATCH COMPARISONS BETWEEN THE PROPOSED AND THE PREVIOUS ALGORITHM

Statistics of Errors	Previous Algorithm [11], [19]	Proposed Algorithm	Change
Minimum Value	0mi	0mi	0%
Maximum Value	1355.28mi	732.40mi	-45.96%
Median Value	92.41mi	83.99mi	-9.11%
Mean Value	154.30mi	128.40mi	-16.79%
Standard Deviation	268.36mi	137.30mi	-48.84%

C. Practical Applications in Actual U.S. Power Systems and Batch Comparisons Between the Proposed and the Previous Algorithms

It should be mentioned that the tests in a large number of cases are also required for comprehensive comparisons. There are total of 100 confirmed cases employed in this section and the results are shown in Fig. 13. It can be seen that both the proposed and previous algorithms can achieve small errors (i.e., <200miles) for most cases and the proposed algorithm is slightly better than the previous one. However, there are large estimation errors for several extreme cases when using the previous algorithm while the proposed algorithm can greatly reduce the estimation errors. The statistics of errors for batch comparisons between the proposed and the previous algorithm are given in Table IV. Note that the case with the largest error (i.e., 10020mi) of the previous algorithm in Fig. 12 is removed for fair comparisons, since this outlier would greatly increase the mean value and standard deviation of the previous algorithm. Even though, it can be seen from Table IV that the proposed hybrid algorithm outperforms the previous one from all aspects. The maximum value, median value and mean value of errors are respectively reduced by 45.96%, 9.11%, and 16.79%, which show the accuracy promotion of the proposed algorithm. The standard deviation of errors is reduced by 48.84%, which indicates the greater robustness of the proposed algorithm.

It should be acknowledged that the maximum error of the proposed algorithm (i.e., 732.40mi) is not acceptable. However, these relatively large errors of the proposed algorithm are associated with the numerical problems in the process of solving linear equations. Concretely, the cause of numerical problems is unsuitable FDRs (e.g., FDRs that are located too close) are selected, which leads to the singularity of matrix **A** in (15).

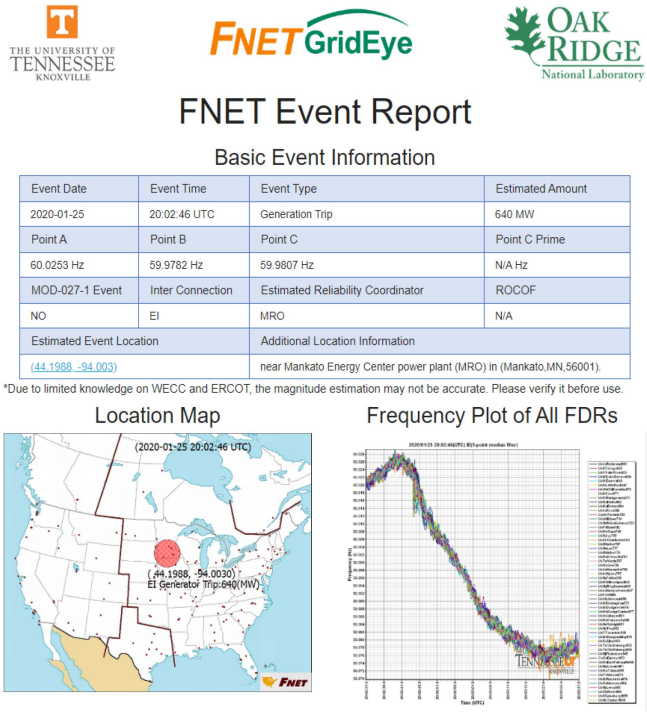

Fig. 14. Event report generated by FNET/GridEye for a given case.

Although few situations with relatively large errors cannot be completely avoided, these situations can be known in advance by checking if the matrix $\mathbf{A}$ in (15) is singular or if the value of residuals in (16) is extremely large. Therefore, corresponding notices can be delivered by the proposed algorithm for the quite inaccurate cases in advance to remind operators it is necessary to verify these results before use.

The event location estimation algorithm has been deployed in FNET/GridEye and an event report with the estimated event location and other critical information can be generated for each detected event in power systems, as shown in Fig. 14.

It is noted that the CNN part is trained by past confirmed events in Python 2.7 environment with 4-fold cross-validation by using GTX 1060 GPU, and the rest parts are implemented in MATLAB 2020a environment with Core i5-7400 CPU and 16GB RAM. The training time for CNN model is 22h16min, the testing time for each case is around 1s. It can be seen that although it cost long time to train the CNN model, the online testing time is quite short. Since the training can be performed in off-line stage, the computation time of the proposed event location estimation algorithm is acceptable in practical application.

V. Discussions

This work aims to propose a practical event location estimation algorithm for applications, therefore, several parameters or thresholds are required to be introduced to deal with various actual situations, and they are determined according to the engineering experience from past events. In fact, if the measured data are ideal, these parameters and thresholds are unnecessary or can be easily selected. However, it makes no sense if the practical situations are not considered. Therefore, it is also significant to study these parameters or thresholds (i.e., N_τ, τ, N_{win}, ζ_1, ζ_2, η) comprehensively for better applications in practice. Concretely, N_τ and τ are associated with the event time determination, which cannot be known very precisely for actual events, therefore, simulated data with noise considered are utilized for the sensitivity analysis for them about event time determination. N_{win}, ζ_1 and ζ_2 are associated with the RoCoF determination and wave arrival time determination. Although it is hard to judge their influence directly, the performance obtained by different values of them can be reflected by the final errors in location estimation. Therefore, the actual measured data are utilized for the sensitivity analysis of N_{win}, ζ_1 and ζ_2. Similarly, although it is hard to evaluate the parameter η directly, the performance obtained by different values of η can be reflected by the final errors in location estimation. Therefore, the actual measured data are utilized for the sensitivity analysis of η as well.

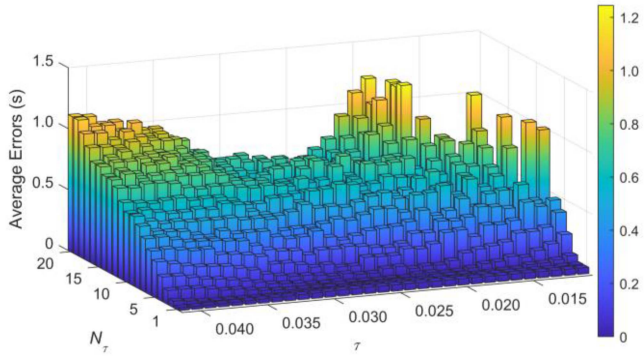

Fig. 15. Result of the sensitivity analysis of N_τ and τ.

It should be clarified that: i) event time cannot be obtained very precisely for actual events but can be obtained for simulated ones, therefore, the first sensitivity analysis needs to be performed by simulated data; ii) simulated data are lack of geographic information (i.e., GPS coordinates), therefore, the last two sensitivity analyses need to be performed by the actual measured data. Furthermore, using actual measured data would be more in line with the actual situation and can test the robustness of the proposed algorithm.

A. Sensitivity Analysis of N_τ and τ for Event Time Determination

N_τ and τ are two parameters for event detection. Concretely, N_τ controls the least number of FDRs receiving disturbance wave can announce an event, and τ controls the weakest wave fluctuation that can announce an event. Small values of N_τ and τ can detect the events more sensitively while it may also cause error detections; on the contrary, large values of N_τ and τ can detect the events more firmly while it may cause missing detections. To study the influence of N_τ and τon event time determination, hundreds of simulated cases are utilized for sensitivity analysis, and the average errors for event time determination are shown in Fig. 15. It should be mentioned that

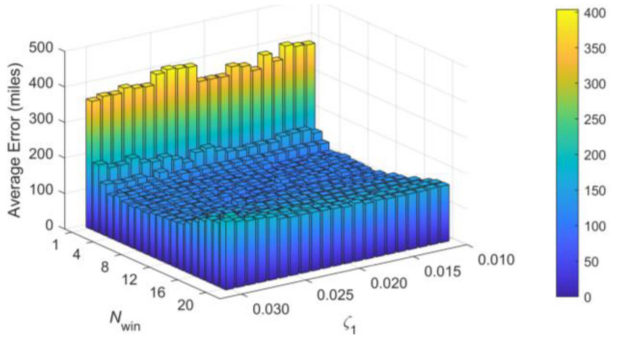

Fig. 16. Result of the sensitivity analysis of $N_{\rm win}$, ζ_1 and ζ_2.

Gaussian noises with 30 dB signal-noise ratio (SNR) were added for the simulated data.

It can be seen from Fig. 15 that the average errors are relatively small when N_τ<5 and 0.020<τ<0.030. Therefore, any values of N_τ and τ that within the above range can be selected for event time determination since the values of the average errors are relatively smaller and stable in this range. In particular, the smallest average error is 0.1735 and is obtained when N_τ= 4 and τ= 0.0221. Therefore, the parameters N_τ= 4 and τ= 0.0221 are employed in this work. It should be clarified that different selections of the parameters N_τ and τ would cause the increase of average errors in this work. However, the differences among errors would not be very large as long as N_τ<5 and 0.020<τ<0.030.

B. Sensitivity Analysis of N_{win}, ζ_1 and ζ_2 for RoCoF Determination and Wave Arrival Time Determination

Due to the measurement noise in actual situations, practicable values of RoCoF cannot be obtained if $N_{\rm win} = 1$, which would cause large errors for event location estimation. Due to the same reason, the parameters ζ_1 and ζ_2 are also introduced to determine the wave arrival time more precisely. Therefore, the sensitivity analysis of $N_{\rm win}$, ζ_1 and ζ_2 is performed in this sub-section, and their influences on the final location estimation errors are shown in Fig. 16. It is noted that ζ_1 and ζ_2 are symmetric variables (i.e., $\zeta_1 = -\zeta_2$) and the values in the x-axis denote the values of ζ_1. It is also worth mentioning that each group of the parameters $N_{\rm win}$, ζ_1 and ζ_2 are tested by all actual measured events mentioned in Section IV–C, and the errors in Fig. 16 are the mean values.

It can be seen that the errors are quite large when $N_{\rm win}$ is smaller than 5 or larger than 15. Although different cases may have the different best selection of ζ_1 and ζ_2, the sensitivity analysis finds that ζ_1 and ζ_2 also have an insensitive interval. The results in Fig. 16 demonstrate that the event location estimation errors are relatively small when ζ_1 is larger than 0.002 or smaller than 0.001. Therefore, as long as $0.001 < \zeta_1 < 0.002$ (i.e., $-0.002 < \zeta_2 < -0.001$), the change of ζ_1 and ζ_2 will not have a large impact on the final event location estimation accuracy.

In summary, the errors in the center of Fig. 16 are relatively small and stable, so the parameters can be selected in this range with no big difference. Hence, $N_{\rm win} = 6$, ζ_1= 0.015, and ζ_2= −0.015 are utilized in the proposed algorithm.

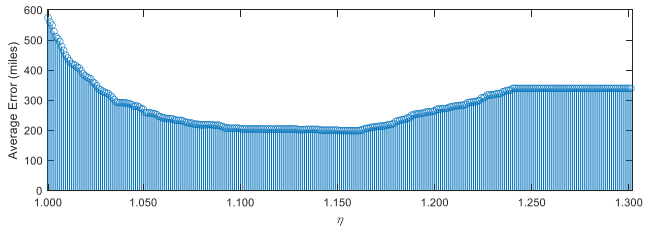

Fig. 17. Result of the sensitivity analysis of η.

C. Sensitivity Analysis of η for the Triggering Condition of Oscillation Intensity Criteria

The parameter η decides whether the oscillation intensity criteria should be used. Similar to Section V–B, the value of η is enumerated and tested by all actual events, and the results are shown in Fig. 17. It can be observed that the errors are very larger on the left side and decrease sharply with the increase of η. However, the errors increase again when η larger than 1.20. The reason is the reliability of oscillation intensity criteria for location estimation is lower than the criteria of wave arrival time (e.g., oscillation may occur far away from the fault source sometimes). Therefore, the errors can be quite large when η is near to 1 (i.e., oscillation intensity criteria would be always triggered). When η is set too large (i.e., >1.2), then the criteria would not be triggered anymore. Therefore, $\eta = 1.15$ is utilized in this work so that the oscillation intensity criteria would only be triggered for auxiliary location estimation when oscillations are large enough.

D. Illustrations About the Practical Significances of FENT/GridEye and the Proposed Event Location Estimation Algorithm

The practical significances of FNET/GridEye and the proposed event location estimation algorithm can be clarified in the following three aspects.

i) The FNET/GridEye is a WAMS network deployed at the distribution level and high dynamic accuracy FDRs are used to measure the frequency, phase angle, and voltage for the U.S. power systems [25], [26]. Compared with transmission-level WAMS and commercial PMUs, the installation density of FDR is much smaller. Therefore, it is unfair to compare the effectiveness of event location estimation between the algorithm using FDR data and the algorithm using PMU or SCADA data. In fact, the proposed algorithm was also tested by using actual PMU data, and the error is 0 for most cases. Hence, it is the limitations of the number of measurement devices and data that cause the relatively large errors, rather than the proposed event location estimation algorithm.

ii) Even though the SCADA system can locate the events more accurately sometimes, the FNET/GridEye also have unique significance under the situations in the U.S. power systems. It should be noted that there are several power utilities in the U.S. and each power utility can only access their own measurement data and do not have an overall

view of the whole power system. In contrast, the measurement data of FNET/GridEye are national-wide and are much easier to access when compared with PMU data. Therefore, the FNET/GridEye can be utilized for global analysis for the U.S. power systems, which is impossible for PMU or SCADA system deployed by different power utilities. For example, a forced oscillation was observed across the entire Eastern Interconnection from 08:44:41 UTC to 09:02:23 UTC on January 11, 2019 [27]. First, Reliability Coordinators (RCs) identified oscillation on PMU data and notified RC Hotline; then FNET/GridEye provided videos of oscillation event [28]; next, the source was tentatively determined as Bayside #2 Steam Unit in Florida; finally, North America Electric Reliability Corporation (NERC) issued PMU data request, worked with possible source, and performed further oscillation analysis on wide-area data set. Therefore, it can be seen that FNET/GridEye and the corresponding event location estimation algorithm play an important role during the actual event identification process. They provide a global view and preliminary location so as to coordinate the further actions among different power utilities, and also to help select critical PMU data required for further analysis.

iii) Traditional event location estimation algorithms using PMU data are generally based on the voltage phase information and they do not rely upon machine learning or deep learning algorithms and do not need huge training data indeed. However, the principle of these traditional algorithms is to determine the event location as the most impact PMU. In such a situation, the estimation results are always one of the deployment locations of PMUs, and the actual event locations cannot be given. The estimation error can be very large if the actual event location is far away from the nearest deployed PMU. In contrast, the proposed event location estimation algorithm can estimate the actual event location based on triangulation, oscillation intensity, and CNN comprehensively. In brief, the traditional algorithms can only give qualitative results while the proposed algorithm can give quantitative results.

VI. Conclusion

In this work, a hybrid event location estimation algorithm is proposed, which can be divided as three aspects: i) phase angle and RoCoF trajectories are used to determine the wave arrival time; ii) CNN is used to determine the wave arrival order so as to modify the wave arrival time determined in i) for triangulation; and iii) COI phase angle trajectories are used for determining the oscillation intensity. The proposed hybrid algorithm is illustrated by two typical events cases and also verified by numerous actual and confirmed cases in the U.S. power systems. Compared with the existing event location estimation algorithm, the proposed one can achieve much fewer estimation errors, especially for the extreme cases in practical applications.

It should be mentioned that the wave propagation speed is assumed uniform so that the triangulation equations can be solved successfully with enough conditions in this work. However, the system frequency wave is an electromechanical wave and its propagation speed is different at different directions in fact, which might lead to certain estimation errors. and is also an obstacle for several years. Besides, the FDR can achieve a 10Hz reporting rate and better performance is expected to be achieved once the better instrumentations with a much higher reporting rate (1.44kHz) [29] developed by UTK are widely deployed. Therefore, how to consider the influence of the anisotropy of frequency waves and how to utilize the more advanced instrumentation to achieve better performance will be further studied in our future work.

Acknowledgment

The authors would like to thank all of the FDR host universities, companies, high schools and individuals in the world. North American Electric Reliability Corporation (NERC) also provided help for determining the true event locations.

References

[1] B. Mohandes, M. S. E. Moursi, N. Hatziargyriou, and S. E. Khatib, "A review of power system flexibility with high penetration of renewables," *IEEE Trans. Power Syst.*, vol. 34, no. 4, pp. 3140–3155, Jul. 2019.

[2] H. Xiao, K. Sun, J. Pan, Y. Li, and Y. Liu, "Review of hybrid HVDC systems combining line communicated converter and voltage source converter," *Int. J. Elect. Power Energy Syst.*, vol. 129, no. 2, Art. no. 106713.

[3] S. Liu *et al.*, "Robust system separation strategy considering online wide-area coherency identification and uncertainties of renewable energy sources," *IEEE Trans. Power Syst.*, vol. 35, no. 5, pp. 3574–3587, Sep. 2020.

[4] H. Liu *et al.*, "Impacts of subsynchronous and supersynchronous frequency components on synchrophasor measurements," *J. Modern Power Syst. Clean Energy*, vol. 4, no. 3, pp. 362–369, Jul. 2016.

[5] W. Yao, L. Zhan, H. Yin, and Y. Liu, "PMU holdover performance enhancement using double-oven controlled oscillator," *IEEE Trans. Power Del.*, vol. 34, no. 6, pp. 2260–2262, Dec. 2019.

[6] K. Sun *et al.*, "WAMS-based HVDC damping control for cyber attack defense," *IEEE Trans. Power Syst.*, to be published, doi: 10.1109/TPWRS.2022.3168078.

[7] Y. Liu *et al.*, "Recent developments of FNET/GridEye — A situational awareness tool for smart grid," *CSEE J. Power Energy Syst.*, vol. 2, no. 3, pp. 19–27, Sep. 2016.

[8] Y. Liu *et al.*, "Wide-area measurement system development at the distribution level: An FNET/GridEye example," *IEEE Trans. Power Del.*, vol. 31, no. 2, pp. 721–731, Apr. 2016.

[9] W. Li, J. Tang, J. Ma, and Y. Liu, "Online detection of start time and location for hypocenter in north America power grid," *IEEE Trans. Smart Grid*, vol. 1, no. 3, pp. 253–260, Dec. 2010.

[10] J. Zuo, M. Baldwin, H. Zhang, J. Dong, K. S. Kook, and Y. Liu, "Use of frequency oscillations to improve event location estimation in power systems," in *Proc. IEEE Power Eng. Soc. Gen. Meeting*, Tampa, FL, USA, 2007, pp. 1–7.

[11] T. Xia *et al.*, "Wide-area frequency based event location estimation," in *Proc. IEEE Power Eng. Soc. Gen. Meeting*, Tampa, FL, USA, 2007, pp. 1–7.

[12] K. Kook and Y. Liu, "Wide-area frequency-based tripped generator locating method for interconnected power system," *J. Elect. Eng. Technol.*, vol. 6, no. 3, pp. 776–785, 2011.

[13] P. Bhui and N. Senroy, "Application of recurrence quantification analysis to power system dynamic studies," *IEEE Trans. Power Syst.*, vol. 31, no. 1, pp. 581–591, Jan. 2016.

[14] Y. Seyedi, H. Karimi, and S. Grijalva, "Irregularity detection in output power of distributed energy resources using PMU data analytics in smart grids," *IEEE Trans. Ind. Inform.*, vol. 15, no. 4, pp. 2222–2232, Apr. 2019.

[15] S. Liu *et al.*, "Data-driven event detection of power systems based on unequal-interval reduction of PMU data and local outlier factor," *IEEE Trans. Smart Grid*, vol. 11, no. 2, pp. 1630–1643, Mar. 2020.

[16] C. F. Karney, "Transverse Mercator with an accuracy of a few nanometers," *J. Geodesy*, vol. 85, no. 8, pp. 475–485, 2011.
[17] K. Kawase, "Concise derivation of extensive coordinate conversion formulae in the Gauss-Krüger projection," *Bull. Geospatial Inf. Authority Jpn.*, vol. 60, pp. 1–6, 2012.
[18] D. Zhou *et al.*, "Distributed data analytics platform for wide-area synchrophasor measurement systems," *IEEE Trans. Smart Grid*, vol. 7, no. 5, pp. 2397–2405, Sep. 2016.
[19] Y. Ye, "Wide-area situation awareness application developments," Ph.D. dissertation, Dept. Elect. Eng. Comput. Sci., The Univ. Tennessee, Knoxville, TN, USA, 2011.
[20] S. You *et al.*, "Calculate center-of-inertia frequency and system RoCoF using PMU data," in *Proc. IEEE Power Eng. Soc. Gen. Meeting*, Washington, DC, USA, 2021, pp. 1–5.
[21] P. Gupta, R. S. Bhatia, and D. K. Jain, "Active ROCOF relay for islanding detection," *IEEE Trans. Power Del.*, vol. 32, no. 1, pp. 420–429, Feb. 2017.
[22] W. Wang *et al.*, "Frequency disturbance event detection based on synchrophasors and deep learning," *IEEE Trans. Smart Grid*, vol. 11, no. 4, pp. 3593–3605, Jul. 2020.
[23] S. Liu *et al.*, "Data-driven event identification in the U.S. power systems based on 2D-OLPP and RUSBoosted trees," *IEEE Trans. Power Syst.*, vol. 37, no. 1, pp. 94–105, Jan. 2022.
[24] N. B. Shah and M. J. Wainwright, "Simple, robust and optimal ranking from pairwise comparisons," *J. Mach. Learn. Res.*, vol. 18, no. 1, pp. 7246–7283, Apr. 2017.
[25] Y. Liu *et al.*, "Wide-area-measurement system development at the distribution level: An FNET/GridEye example," *IEEE Trans. Power Del.*, vol. 31, no. 2, pp. 721–731, Apr. 2016.
[26] "FNET/GridEye web display," Accessed: Jan. 25, 2022. [Online]. Available: http://fnetpublic.utk.edu/index.html
[27] "January 11, 2019 eastern interconnection forced oscillation event," Accessed: Jan. 25, 2022. [Online]. Available: https://www.nerc.com/pa/rrm/ea/Pages/Oscillation-Event-Report.aspx
[28] "20190111-084423_EI_Non-obvious Event," Accessed: Jan. 25, 2022. [Online]. Available: https://www.youtube.com/watch?v=xilfYKxqEDo
[29] H. Yin, W. Yu, A. Bhandari, W. Yao, and L. Zhan, "Advanced universal grid analyzer development and implementation," in *Proc. Int. Conf. Smart Grid Synchronized Meas. Analytics*, College Station, TX, USA, 2019, pp. 1–5.